# OBSERVATION CRITERIA TRADE-OFF FOR GEO DEBRIS CATALOGUING

**D. Gil Calvo[1], P. Diaz Morales[2], G. Principe[3], A. Mazzoleni[4]**

[1] *Indra-Deimos, Ronda de Poniente 19 – 28760 Tres Cantos, Madrid (Spain), Email: dgilc@indra.es*
[2] *Indra-Deimos, Ronda de Poniente 19 – 28760 Tres Cantos, Madrid (Spain), Email: pdmorales@indra.es*
[3] *Indra-Deimos, Ronda de Poniente 19 – 28760 Tres Cantos, Madrid (Spain), Email: gprincipe@indra.es*
[4] *Indra-Deimos, Ronda de Poniente 19 – 28760 Tres Cantos, Madrid (Spain), Email: amazzoleni@indra.es*

## ABSTRACT

In recent years, the rise in space occupancy has become a main concern for the international space community. An uncontrolled growth of the space population could lead to undesirable situations such as break-ups or collisions which would increase the threat even more. In this context, the cataloguing of the space objects becomes crucial in order to ensure safe space operations, especially when dealing with collision avoidance between operative and non-operative (debris) objects.

The number of sensors tracking space objects all over the world has increased, as it is evidenced by the growth of the commercial ones. However, the observation resources are still limited (e.g. optical sensors can observe only during the night, and radars are expensive technologies), hence the observation of the space debris must be optimized to guarantee a correct object cataloguing with the minimum sensor time dedication. Too frequent observations of an object may not result in a major improvement of the computed ephemeris accuracy, while an insufficient tracking would lead to imprecise orbit computation. Precision in the determined orbits is a key factor and cannot be neglected, as it facilitates the correlation of successive observations, allowing the automatization of the space cataloguing service.

Particularly speaking about GEO debris, the precision in cataloguing depends on four key factors: the selected orbit determination method, the precision of the supporting sensor network, the number of object measurements and the distribution of those measurements along the orbit. This study focuses on the analysis of the impact of the two latter factors on the computed orbital precision using the measurements taken by a real optical sensor and the Batch-Least Squares as orbit determination (OD) method. First, different observation scenarios are considered by varying number and distribution of the measurements to be used for the OD. The resulting ephemerides are then compared to a reliable external catalogue (i.e. SP catalogue) in order to quantify their precision. The objective of the analysis is to define a strategy for the sensors' planification focusing on lowering sensor time usage while guaranteeing the desired ephemeris precision. Finally, the automatic and autonomous catalogue maintenance is assessed by ensuring the correct correlation of successive tracks to well-catalogued objects, following the observation scenarios considered in the previous section.

In conclusion, by analysing the impact of measurement number and distribution on orbital precision, we show that a careful balance must be struck between frequent tracking and computational efficiency. These findings contribute to the development of autonomous space debris management systems, ensuring safer and more sustainable operations in Earth's orbital environment.

## 1 INTRODUCTION

Space debris, consisting of defunct satellites, spent rocket stages, and fragments from collisions, poses a significant threat to operational spacecrafts. These objects travel at high velocities, increasing the risk of catastrophic collisions that can damage or destroy satellites and other space assets. The growing number of debris objects in orbit has led to concerns about the sustainability of space activities and the potential for a cascading effect known as the Kessler Syndrome, where collisions generate more debris, further increasing collision risks.

To mitigate these risks, it is crucial to maintain an accurate catalogue of space objects. Cataloguing involves detecting, tracking, and identifying all objects in orbit, providing essential data for collision avoidance and space traffic management. This information helps satellite operators plan manoeuvres to avoid collisions and ensures the safety of both manned and unmanned missions. Effective cataloguing is fundamental to preserving the long-term usability of the space environment.

Given the vast number of objects in orbit, optimized tracking strategies are necessary to efficiently monitor and manage space debris. Traditional tracking methods may not be sufficient to handle the increasing volume and complexity of space traffic. Advanced technologies and innovative approaches are then required to enhance tracking accuracy, reduce uncertainties, and improve the reliability of collision predictions. Optimized tracking strategies are also a relevant factor that can significantly reduce operational costs and enhance the safety of space

*Proc. 9th European Conference on Space Debris, Bonn, Germany, 1–4 April 2025, published by the ESA Space Debris Office*
*Editors: S. Lemmens, T. Flohrer & F. Schmitz, (http://conference.sdo.esoc.esa.int, April 2025)*

missions.

This study aims to explore the trade-offs involved in observation criteria for cataloguing geostationary orbit (GEO) debris. By analysing different observation scenarios, the goal is to minimize the time a sensor spends observing a single object while ensuring its correct cataloguing.

## 2 KEY FACTOR INFLUENCING GEO DEBRIS CATALOGUING

The effective cataloguing of GEO debris is essential for maintaining the safety and sustainability of space operations. Several key factors influence the accuracy and reliability of debris catalogues, each playing a crucial role in the overall process. Here three main factors are analysed: orbit determination (OD) methods, sensor network configuration, and measurement frequency and distribution. Understanding and optimizing these factors are key for enhancing the precision of debris tracking.

### 2.1 Orbit Determination Methods

OD is a fundamental process in GEO debris cataloguing, providing estimates of an object’s trajectory based on available measurements. Several computational methods exist, each offering different advantages depending on the availability of data, required accuracy, and computational constraints.

A key distinction in OD approaches lies between batch processing and sequential estimation. Batch processing involves collecting a set of observations over a period and processing them simultaneously to estimate the object’s state. This approach provides a more stable and accurate solution, as it incorporates all available data at once, minimizing random errors. However, it requires a sufficient number of observations before computation, making it less suited for real-time applications. If too few observations are used, the estimated orbit may be highly sensitive to measurement noise, resulting in a less accurate trajectory. In contrast, sequential estimation updates the orbit progressively as new measurements become available. Techniques such as the Kalman filter, along with its variations (e.g., extended or unscented Kalman filters), allow real-time refinement of an object's trajectory. This makes sequential methods particularly useful for continuous tracking and adaptive catalogue maintenance.

Within batch processing, least-squares (LS) estimation is a widely used mathematical technique for fitting an orbit to observational data. This method minimizes the residuals between observed and computed data, ensuring the best possible trajectory estimate. A more common variant is the weighted LS, which accounts for differences in measurement uncertainties, improving robustness.

The choice of OD method depends on the specific requirements of GEO debris cataloguing. Batch processing with LS estimation is often preferred for high-precision OD when sufficient data is available, while sequential methods like the Kalman filter are more suitable for real-time tracking and catalogue updates. In many cases, a combination of approaches is employed to ensure both initial orbit acquisition and long-term refinement, supporting the accurate and reliable tracking of GEO debris.

### 2.2 Sensor network

The configuration of the sensor network is a critical factor in the effectiveness of GEO debris cataloguing. A well-designed sensor network ensures comprehensive coverage, continuous monitoring, and accurate data collection, which are essential for maintaining an up-to-date and reliable debris catalogue.

Ground-based sensors, such as optical telescopes and radar systems, form the backbone of many space surveillance networks. Optical telescopes are particularly effective for observing GEO debris due to their ability to cover large areas of the sky and detect objects at great distances. These telescopes can provide high-resolution images that help in identifying and tracking debris objects. The main problem with telescopes is that they are unable to make observations during daylight or in poor weather conditions.

A well-distributed network of sensors ensures that space objects are observed from multiple angles and at different times, providing a more comprehensive dataset for OD. This helps in reducing the uncertainties associated with single-sensor observations and enhances the overall accuracy of the debris catalogue.

As the number of space objects continues to increase significantly, the availability of telescopes remains limited. This constraint makes it essential to optimize both the time allocated for observations and the overall observation planning to ensure efficient tracking and catalogue maintenance.

### 2.3 Measurement frequency and distribution

The frequency and distribution of measurements are key factors in the effective cataloguing of GEO debris. They influence the accuracy of the OD and, in turn, the reliability and timeliness of the catalogue.

Frequent observations are necessary to track the dynamic nature of space debris and to update their orbits regularly, maintaining the accuracy of the catalogue by reducing the uncertainties in the predicted orbits.

The distribution of observations across different observation times is also important for improving the precision of orbit predictions. The strategic distribution of observation times ensures continuous debris monitoring, allowing observations to cover a larger portion of the orbit and improving the accuracy of the OD solution. This is crucial because, when observations are spread over a short arc, only partial information about the curvature of the orbit can be inferred and, thus, the estimated orbit will be affected by a large uncertainty [1].

## 3 METHODOLOGY

This section describes the implemented methodology. It begins with an overview of the data and the algorithm used for OD, followed by the definition of the observational scenarios and the criteria for evaluating each one.

This study focuses on the last factor discussed in the previous section: the impact of measurement frequency and distribution on the OD process. To address this, a weighted LS approach has been selected, processing observations collected from a single telescope.

### 3.1 Data Collection

In this analysis, real data from the survey sensor CENTU2, collected in early March 2025 for three different debris objects, were processed using the OD algorithm. Debris objects were selected instead of active satellites to avoid potential manoeuvres that could impact OD accuracy. CENTU2, operated by Indra-Deimos, is located in El Sauce Observatory (Obstech, Chile). It provides a southern and western view of the sky, as well as enjoying of a superb seeing. The resulting measurements present an accuracy higher than 1.4 arcseconds, which implies a precision in the GEO ring of ~250m.

The selected debris objects for the analysis are:

- GORIZONT 6 (NORAD: 13624)
- COSMOS 2629 (NORAD: 15574)
- COSMOS 2054 (NORAD: 20391)

In this analysis, each retrieved track, consisting of a set of sequential observations, includes four observations approximately 2.5 seconds apart. The overall observation window was carefully selected to ensure that the three objects were observed with sufficient frequency, allowing for the construction of multiple observation scenarios by combining the retrieved tracks.

### 3.2 Batch-Least Squares Orbit Determination Method

For the sake of completeness, here a brief description of the algorithm used for OD is given. For a given initial condition of a space object, with state $X_{t_0}$, and for an available arc observation, *Batch Least-Squares* (BLS) algorithm provides the best estimate at the epoch state,

$$\hat{X}_{t_0} = X_{t_0} + \delta x_{t_0} \tag{1}$$

This is carried out in an iterative process by solving a normal equation,

$$\delta x_{t_0} = (A^T W A)^{-1} A^T W b \tag{2}$$

where $A$ is the partial derivative matrix, $W$ is the weighting matrix and $b$ represents the residual vector.

The partial derivative matrix, $A$, is usually composed of the observation matrix, $H$, and the state transition matrix $\Phi$,

$$A = \frac{\partial \alpha(t)}{\partial X(t)} \frac{\partial X(t)}{\partial X_{t_0}} = H_{t,t} \Phi_{t_0,t} \tag{3}$$

The $A$ matrix is approximated by using finite differencing.

### 3.3 Scenarios Definition

To assess the impact of the number and distribution of measurements on OD precision, a set of observational scenarios is defined based on different tracking parameters.

These scenarios are characterized by three key factors:

- Observation Window: The total number of nights the satellite is tracked.
- Observation Gaps: The interval between observations, specifically whether the satellite is observed nightly or every two or three nights.
- Observation Frequency: The number of tracks collected per night.

To systematically evaluate these factors, multiple observation scenarios are established by varying each parameter while keeping the others constant:

*Table 1. Definition of observation scenarios.*

| Scenario | Observation Window | Observation Gaps | Observation Frequency |
|---|---|---|---|
| A & B | 7 nights | Nightly | 1 |
| C | 7 nights | Every 2 nights | 1 |
| D | 7 nights | Every 3 nights | 1 |
| E | 7 nights | Nightly | 2 |
| F | 5 nights | Nightly | 1 |
| G | 5 nights | Nightly | 2 |
| H | 3 nights | Nightly | 1 |
| I | 3 nights | Nightly | 2 |

The importance of observing the object covering different part of its orbit is assessed by comparing the Scenarios A and B. In Scenario B, tracks are close to each other and cover only a part of the observation window from the sensor location, which in the case of GEO objects indicates close orbital positions. In contrast, in Scenario A observations are spread over the maximum observation window from the sensor.

To ensure OD convergence and minimize the loss of precision, tracks distributed along the largest portion of the orbital arc have been selected for Scenarios C to I.

### 3.4 Trade-off Criteria

The different scenarios are evaluated based on the accuracy of the resulting ephemerides compared to a reliable external catalogue, the Special Perturbations (SP) High-Accuracy catalogue. The SP ephemerides are derived from a numerical OD process, solved for a high-level force mode and provided daily [2].

The accuracy is computed by means of the $RMS_{3D}$ and Maximum Distance ($MaxD_{3D}$):

$$RMS_{3D} = \sqrt{\Delta_{3D}^2 + SD_{3D}^2} \tag{4}$$

$$MaxD_{3D} = \sqrt{MaxD_{along}^2 + MaxD_{cross}^2 + MaxD_{radial}^2} \tag{5}$$

where

$$\Delta_{3D} = \sqrt{\Delta_{along}^2 + \Delta_{cross}^2 + \Delta_{radial}^2} \tag{6}$$

$$SD_{3D} = \sqrt{SD_{along}^2 + SD_{cross}^2 + SD_{radial}^2} \tag{7}$$

$\Delta_{along}$, $\Delta_{cross}$ and $\Delta_{radial}$ are the average differences between the points of the two orbits being compared (the resulting orbit from the scenario under analysis against the SP orbit). $SD_{along}$, $SD_{cross}$ and $SD_{radial}$ are the standard deviation of the averages mentioned before. $MaxD_{along}$, $MaxD_{cross}$ and $MaxD_{radial}$ are the maximum difference between the points on each direction. The average values are computed using points either from the first orbital period after the OD or from the seventh period. This provides insight into both the accuracy immediately after the OD and the one at the end of the propagation.

## 4 RESULTS

The resulting Key Performance Indicators (KPIs), $RMS_{3D}$ and Maximum Distance of the computed ephemeris in each of the observation scenarios, are reported in ANNEX A. To evaluate the degradation or improvement in orbit accuracy between two scenarios, the ratio of each KPI is computed, using Scenario A (nightly observations over seven days) as the reference. In the analysis of the influence of observation frequency, the ratios are calculated using the one-track-per-night scenario as the reference.

### 4.1 Influence of Tracks Distribution along the Orbit

As stated in [1], the OD solution improves when using observations covering a larger section of the orbit.

The localization of the satellite within its orbit with respect of the sensor position has been characterized using topocentric coordinates, specifically by relating the parameters of right ascension (RA) and declination (DE).

Figure 1, Figure 2 and Figure 3 show the RA vs DE arc covered by the tracks selected for Scenarios A and B. It can be observed that tracks from Scenario B were retrieved from close orbital positions, unlike those in Scenario A, which extend over a larger portion.

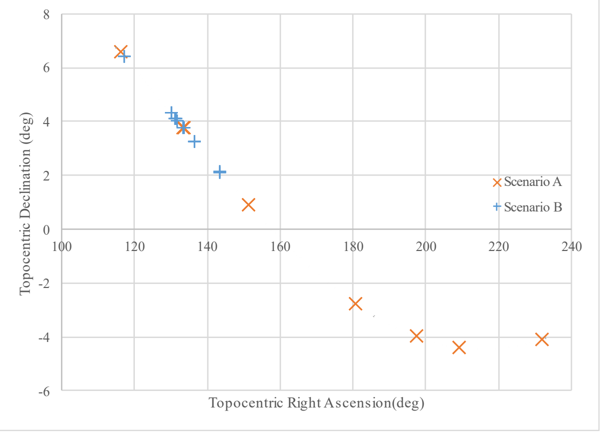


*Figure 1. Topocentric Right Ascension (RA) and Declination (DE) covered by the tracks of Scenarios A and B of GORIZONT 6.*

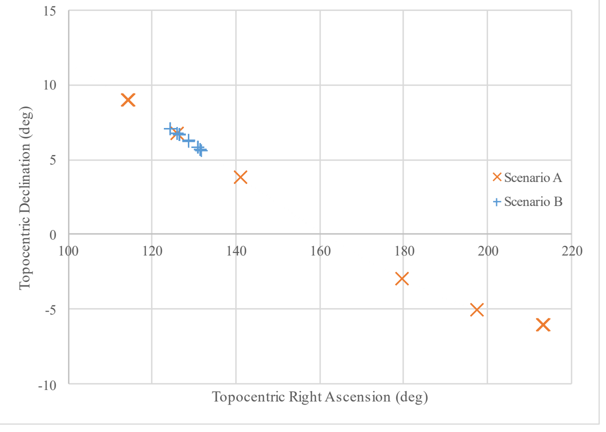


*Figure 2. Topocentric Right Ascension (RA) and Declination (DE) covered by the tracks of Scenarios A and B of COSMOS 2629.*

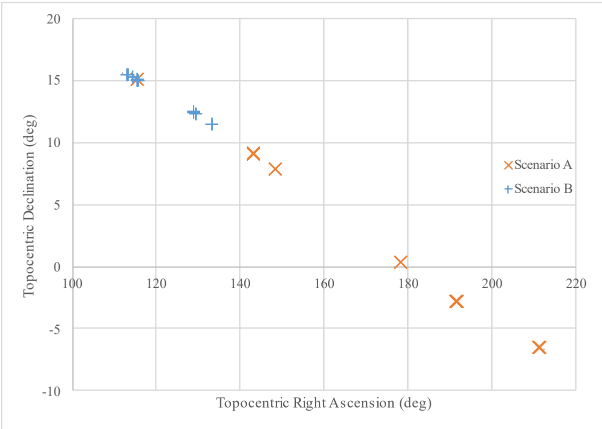


*Figure 3. Topocentric Right Ascension (RA) and Declination (DE) covered by the tracks of Scenarios A and B of COSMOS 2054.*

The computed ephemeris of each scenario has been compared to the corresponding SP orbit, resulting in the KPIs presented in ANNEX A. The ratio between KPIs from the Scenarios B and A is reported in Table 2.

*Table 2. $RMS_{3D}$ and Maximum Distance ratios between Scenarios B and A. Values retrieved for the 1st and 7th revolutions.*

| NORAD | $RMS_{3D}$ ratio | | Max Distance ratio | |
|---|---|---|---|---|
| | 1st Rev | 7th Rev | 1st Rev | 7th Rev |
| 13624 | 39.27 | 32.62 | 39.96 | 31.66 |
| 15574 | Scenario B OD not converged | | | |
| 20391 | 8.32 | 2.49 | 8.22 | 2.51 |

It can be observed that both the $RMS_{3D}$ and maximum distance values increase when using tracks in the same arc positions, ranging from 33 to 40 times higher for GORIZONT 6 (depending on the revolution) and 2 to 8 times higher for COSMOS 2054. Furthermore, the OD process using the COSMOS 2629 tracks of Scenario B failed to converge to a solution.

## 4.2 Influence of Observation Gaps

To quantify the impact of observation gaps on the OD process, Scenarios A, C, and D are compared. The resulting KPIs are presented in Table 3.

*Table 3. $RMS_{3D}$ and Maximum Distance ratios between scenarios depending on the observation gaps. Values retrieved for the 1st and 7th revolutions.*

| NORAD | Compared Scenarios | $RMS_{3D}$ ratio | | Max Distance ratio | |
|---|---|---|---|---|---|
| | | 1st Rev | 7th Rev | 1st Rev | 7th Rev |
| 13624 | C / A | 10.94 | 18.13 | 11.46 | 17.95 |
| | D / A | Scenario D OD not converged | | | |
| 15574 | C / A | 8.20 | 10.81 | 8.43 | 10.98 |
| | D / A | Scenario D OD not converged | | | |
| 20391 | C / A | 1.56 | 1.33 | 1.60 | 1.36 |
| | D / A | 3.30 | 0.94 | 3.41 | 0.92 |

The results show that the lack of observations in a night (C / A) leads to a worsening of the computed ephemeris, reaching degradations up to 11 times in the case of the GORIZONT 6.

The lack of observations during two consecutive nights results in no convergence of the OD for two of the cases.

Finally, the observed decrease in $RMS_{3D}$ and maximum distance values during the 7th revolution compared to the 1st revolution for COSMOS 2054 requires further investigation. Additional analysis is necessary to determine whether the counterintuitive result is justified by the propagation conditions.

## 4.3 Influence of Observation Window

The observation window needed to ensure a precise OD solution is assessed by comparing Scenarios A, F and H.

*Table 4. $RMS_{3D}$ and Maximum Distance ratios between scenarios depending on the observation window. Values retrieved for the 1st and 7th revolutions.*

| NORAD | Compared Scenarios | $RMS_{3D}$ ratio | | Max Distance ratio | |
|---|---|---|---|---|---|
| | | 1st Rev | 7th Rev | 1st Rev | 7th Rev |
| 13624 | F / A | 4.71 | 12.32 | 4.97 | 12.27 |
| | H / A | 17.95 | 22.56 | 18.14 | 20.26 |
| 15574 | F / A | 1.56 | 2.00 | 1.55 | 1.98 |
| | H / A | 5.05 | 14.49 | 4.78 | 13.87 |
| 20391 | F / A | 0.61 | 0.68 | 0.63 | 0.69 |
| | H / A | 1.50 | 2.10 | 1.59 | 2.21 |

The results indicate that extending the observation period generally improves the accuracy of the generated ephemeris. However, the improvement is significantly greater when increasing the observation window from 3 to 5 nights than from 5 to 7 nights.

Once again, the observed decrease in $RMS_{3D}$ and Maximum Distance values when using a 5-night observation window instead of 7 nights for COSMOS 2054 warrants further investigation. Given that the same object also exhibited anomalous behaviour when assessing the influence of observation gaps, it is possible that an irregularity occurred either during the data collection process or in the propagation conditions.

### 4.4 Influence of Observation Frequency

Finally, the impact of observing the object once or twice per night is evaluated across the three observation window scenarios (3, 5 and 7 nights).

*Table 5. $RMS_{3D}$ and Maximum Distance ratios between scenarios depending on the observation frequency per night. Values retrieved for the 1st and 7th revolutions.*

| NORAD | Compared Scenarios | $RMS_{3D}$ ratio | | Max Distance ratio | |
|---|---|---|---|---|---|
| | | 1st Rev | 7th Rev | 1st Rev | 7th Rev |
| 13624 | E / A | 1.05 | 0.35 | 1.07 | 0.33 |
| | G / F | 0.13 | 0.08 | 0.11 | 0.08 |
| | I / H | 0.1 | 0.14 | 0.06 | 0.13 |
| 15574 | E / A | 0.17 | 0.13 | 0.16 | 0.12 |
| | G / F | 0.26 | 0.09 | 0.24 | 0.08 |
| | I / H | 0.41 | 0.26 | 0.45 | 0.28 |
| 20391 | E / A | 0.16 | 0.25 | 0.16 | 0.25 |
| | G / F | 0.74 | 0.42 | 0.71 | 0.43 |
| | I / H | 0.18 | 0.16 | 0.15 | 0.11 |

Most of the computed ratios show a great improvement of the precision of the generated ephemeris when the object is observed twice per night. In fact, the KPIs presented in ANNEX A show that the Scenario E achieves precision levels close to that of the sensor for all three objects.

It is worth noting that the ratio for GORIZONT 6 between Scenarios E and A during the first revolution is greater than 1, as Scenario A already reaches the sensor's precision.

## 5 CONCLUSIONS

The analysis of various observational scenarios provides valuable insights into how a sensor's time allocation can be optimized to ensure sufficient observation of a space object for generating a precise ephemeris.

It has been demonstrated that when the object is observed only in the same orbital arc positions, the precision of the generated ephemeris decreases significantly compared to scenarios where observations are distributed over a larger portion of the orbit.

Continuous observation of the object is also crucial for ensuring accurate ephemeris generation, since the absence of observations for even a single night can lead to a substantial degradation in the computed OD.

The duration of the observation window plays a key role in improving the accuracy of the generated ephemeris, with satisfactory results achieved when the observation window is at least five nights. Additionally, observing the object twice per night results in significant improvements in OD accuracy across all tested observation windows.

In particular, the scenario with a seven-night consecutive observation window, combined with twice-nightly observations, shows precision levels approaching the sensor's inherent accuracy for all three objects. Extending the sensor's observation time for these objects beyond this point would be inefficient and unnecessary.

One potential direction for future improvements in this analysis is the creation of additional observation scenarios, incorporating more combinations of the factors considered and expanding the analysis to include more objects. This would allow for a more realistic determination of the optimized sensor allocation for observing a single object. Furthermore, the use of multiple sensors positioned at strategic locations around the globe could be explored to assess its impact on the observation of the orbital arc and, consequently, on the precision of the computed ephemeris.

## 6 ANNEX A

The comparison between the computed ephemeris of each scenario and the corresponding SP orbit is reported in Table 6 (GORIZONT 6), Table 7 (COSMOS 2629) and Table 8 (COSMOS 2054).

*Table 6. $RMS_{3D}$ values and Maximum Distance obtained by comparison between the computed ephemeris of each scenario and the SP orbit of GORIZONT 6 (NORAD 13624). Values retrieved for the $1^{st}$ and $7^{th}$ revolutions.*

| Scenario | $RMS_{3D}$ [km] | | Max Distance [km] | |
|---|---|---|---|---|
| | 1st Rev | 7th Rev | 1st Rev | 7th Rev |
| A | 0.249 | 0.414 | 0.396 | 0.693 |
| B | 9.778 | 13.504 | 15.826 | 21.939 |
| C | 2.724 | 7.507 | 4.54 | 12.439 |
| D | OD Not Converged | | | |
| E | 0.262 | 0.146 | 0.425 | 0.227 |
| F | 1.174 | 5.101 | 1.97 | 8.503 |
| G | 0.149 | 0.424 | 0.224 | 0.7 |
| H | 4.469 | 9.338 | 7.184 | 14.037 |
| I | 0.451 | 1.286 | 0.649 | 1.787 |

*Table 7. $RMS_{3D}$ values and Maximum Distance obtained by comparison between the computed ephemeris of each scenario and the SP orbit of COSMOS 2629 (NORAD 15574). Values retrieved for the $1^{st}$ and $7^{th}$ revolutions.*

| **Scenario** | **$RMS_{3D}$ [km]** | | **Max Distance [km]** | |
|---|---|---|---|---|
| | **$1^{st}$ Rev** | **$7^{th}$ Rev** | **$1^{st}$ Rev** | **$7^{th}$ Rev** |
| A | 1.857 | 3.098 | 3.023 | 5.06 |
| B | OD Not Converged | | | |
| C | 15.227 | 33.499 | 25.484 | 55.577 |
| D | OD Not Converged | | | |
| E | 0.324 | 0.392 | 0.486 | 0.608 |
| F | 2.894 | 6.207 | 4.689 | 9.998 |
| G | 0.746 | 0.537 | 1.117 | 0.773 |
| H | 9.378 | 44.897 | 14.441 | 70.182 |
| I | 3.884 | 11.611 | 6.55 | 19.464 |

*Table 8. $RMS_{3D}$ values and Maximum Distance obtained by comparison between the computed ephemeris of each scenario and the SP orbit of COSMOS 2054 (NORAD 20391). Values retrieved for the $1^{st}$ and $7^{th}$ revolutions.*

| **Scenario** | **$RMS_{3D}$ [km]** | | **Max Distance [km]** | |
|---|---|---|---|---|
| | **$1^{st}$ Rev** | **$7^{th}$ Rev** | **$1^{st}$ Rev** | **$7^{th}$ Rev** |
| A | 1.992 | 6.17 | 3.269 | 9.992 |
| B | 16.57 | 15.37 | 26.874 | 25.066 |
| C | 3.104 | 8.182 | 5.216 | 13.632 |
| D | 6.572 | 5.78 | 11.146 | 9.239 |
| E | 0.317 | 1.528 | 0.537 | 2.453 |
| F | 1.215 | 4.211 | 2.066 | 6.924 |
| G | 0.901 | 1.76 | 1.464 | 2.981 |
| H | 2.984 | 12.963 | 5.189 | 22.054 |
| I | 0.536 | 2.093 | 0.778 | 2.335 |

## REFERENCES


[1] G. Principe, R. Armellin and P. Di Lizia, “Nonlinear representation of the confidence region of orbits determined on short arcs,” *Celestial Mechanics and Dynamical Astronomy,* 2019.

[2] E. Stevenson and L. S. S. J. , “Deriving a unified space object catalogue for the purpose of space debris monitoring and modelling,” in *1st NEO and Debris Detection Conference*, Darmstadt, Germany, 2019.